Int. J. Electrochem. Sci., 8 **(2013)** 1026 - 1040

International Journal of
ELECTROCHEMICAL
SCIENCE
www.electrochemsci.org

Electrochemical Properties of $Li_4Ti_5O_{12}$–SnO_2 Composite Powders Prepared by Scalable Spray Drying Process

Kwang Min Yang[1], *Young Jun Hong*[1], *Seung Ho Choi*[1], *Byung Kyu Park*[2], *Yun Chan Kang*[1,*]

[1]Department of Chemical Engineering, Konkuk University, 1 Hwayang-dong, Gwangjin-gu, Seoul 143-701, Korea
[2]Suncheon Center, Korea Basic Science Institute, Suncheon 540-742, Korea
*E-mail: yckang@konkuk.ac.kr

Received: 14 November 2012 / *Accepted:* 11 December 2012 / *Published:* 1 January 2013

Spherical $Li_4Ti_5O_{12}$-SnO_2 composite powders are prepared using scalable spray drying process from a homogeneous aqueous solution. The composite powders exhibit phase purity, compositional homogeneity, unique morphology, and mixed crystal structures consisting of spinel $Li_4Ti_5O_{12}$ and rutile SnO_2 without any impurities. Nanosized SnO_2 crystals are uniformly distributed throughout the spinel $Li_4Ti_5O_{12}$ matrix. The composite powders prepared from the spray solution with 20 wt% excess Li exhibit high initial charge and discharge capacities, 639 and 439 mAh g^{-1}, respectively, in which the Coulombic efficiency is 69%. The discharge capacity of the composite powders decreases from 439 to 359 mAh g^{-1} by the 30th cycle at a current density of 170 mA g^{-1}, the capacity retention being 82%. The presence of $Li_4Ti_5O_{12}$ phase decreases the degree of aggregation of the active Sn powders imbedded in the composite powder matrices during cycling. The stable $Li_4Ti_5O_{12}$ matrix and hollow inner structure of the composite powders also decrease the amount of internal stress due the changes in volume in the composite powder particles during Li intercalation and deintercalation.

Keywords: lithium titanate; tin oxide; spray drying; composite powders; electrochemical properties

1. INTRODUCTION

Spinel $Li_4Ti_5O_{12}$ is a promising candidate for use as anode for Li-ion batteries because it exhibits good Li-ion intercalation and deintercalation reversibility and because it does not exhibit structural change during charge-discharge cycling [1,2]. However, $Li_4Ti_5O_{12}$ exhibits low capacity and poor rate capability because of its low conductivity. $Li_4Ti_5O_{12}$-based composite materials have been studied to obtain anode materials with high capacities and good cycle properties [3-9]. $Li_4Ti_5O_{12}$-SnO_2 (or Sn) composite powders have been synthesized using various methods including high-energy

mechanical milling, sol-gel, and solution precipitation [7-9]. Xiong *et al*. used the sol-gel method to prepare a core-shell-structured SnO_2-$Li_4Ti_5O_{12}$ composite [7] that delivered a reversible capacity of 689 mAh g^{-1} at 0.1 *C*, and 93.4% of that was retained after 60 cycles at 0.2 *C*. The $Li_4Ti_5O_{12}$-SnO_2 composite material prepared using solution precipitation increased the reversible capacity of $Li_4Ti_5O_{12}$ and exhibited good cycling reliability [8]. In the composite material, SnO_2 acted as a bridge between the spinel particles to reduce the interparticle resistance and as a good material for Li intercalation/deintercalation. The $Li_4Ti_5O_{12}$/Sn 10% composite material prepared using high-energy mechanical milling delivered a stable and enhanced discharge capacity of 200 mAh g^{-1} [9]. The electrochemical performances of $Li_4Ti_5O_{12}$/Sn nanocomposites were associated with the size and distribution of the Sn particles in the $Li_4Ti_5O_{12}$ matrix. The smaller the size and the more homogeneous the dispersion of the Sn particles in the $Li_4Ti_5O_{12}$ matrix, the better the cycling performance the $Li_4Ti_5O_{12}$/Sn composites exhibited as compared to bare $Li_4Ti_5O_{12}$ and Sn particles. However, according to previous reports, the $Li_4Ti_5O_{12}$-SnO_2 (or Sn) composite powders were not formed from a homogeneous aqueous solution; $Li_4Ti_5O_{12}$ or SnO_2 powders were used as colloidal seed material to prepare the composite powders.

The microstructures of composite powders strongly affect the electrochemical properties of anode materials that exhibit large changes in volume during cycling. The hollow and yolk-shell structures were mainly studied to prepare anode materials with good cycling properties [10-14]. The hollow voids acted as a buffer layer against alloy expansion during Li intercalation/deintercalation. Although several previous studies have sought to modify the microstructures of Sn-based materials by developing appropriate synthesis routes [15-18], to the best of our knowledge, microstructure-controlled $Li_4Ti_5O_{12}$-SnO_2 composite powders have not been prepared yet from a homogeneous aqueous solution. In this study, spherical, hollow $Li_4Ti_5O_{12}$-SnO_2 composite powders were prepared using scalable spray-drying process from the aqueous spray solution. The electrochemical properties of the $Li_4Ti_5O_{12}$ powders with uniformly distributed SnO_2 were investigated.

2. EXPERIMENTAL

A schematic diagram of spray-drying is shown in Fig. 1. An aqueous spray solution is pumped to a pneumatic atomizing nozzle in order to form droplets several tens of micrometers in diameter. The droplets meet a stream of hot air and lose their moisture very rapidly while remaining suspended in the drying air. The dry powder is separated from the moist air in cyclone by applying centrifugal action. The temperatures of the inlet and outlet of the spray dryer were 350 and 150°C, respectively. The spray solution was prepared by dissolving a stoichiometric ratio of Li nitrate ($LiNiO_3$, Aldrich), titanium tetraisopropoxide (TTIP, $Ti(OCH(CH_3)_2)_4$, Junsei) and tin oxalate (SnC_2O_4, Aldrich) in distilled water with an appropriate amount of nitric acid. The overall concentration of the Li, Ti, and Sn components was 0.5 M. The concentration of citric acid used as the chelating agent was 0.5 M. The precursor powders obtained using spray drying process were post-treated at temperatures between 700 and 1000°C for 10 h in air. The yield of the $Li_4Ti_5O_{12}$-SnO_2 composite powders calculated on the basis of the amount of the post-treated final product was 400 g h^{-1}.

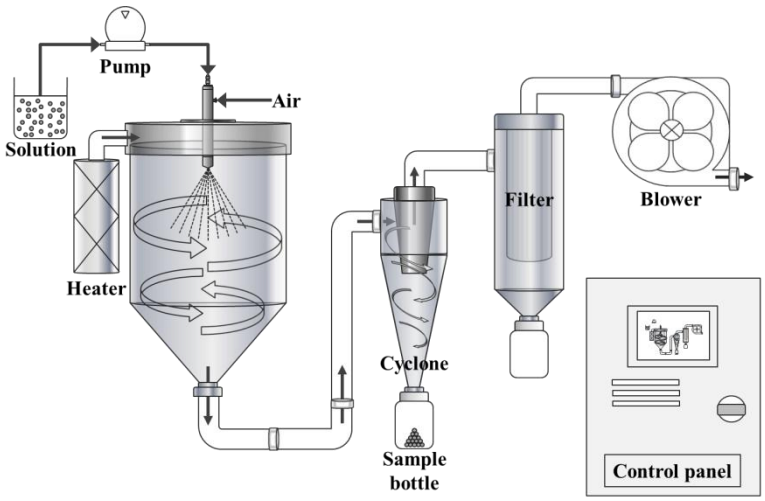

Figure 1. The schematic diagram of the spray drying process.

The crystal structures of the post-treated composite powders were investigated using X-ray diffractometry (XRD, Rigaku DMAX-33) at the Korea Basic Science Institute (Daegu). The morphological characteristics of the powders were investigated using scanning electron microscopy (SEM, JEOL JSM-6060) and transmission electron microscopy (TEM, JEOL JEM-2010). The thermal properties of the precursor powders were investigated using thermogravimetric analysis and differential scanning calorimetry (TGA-DSC) in the range 40–600°C (heating rate: 10°C min^{-1}) with a thermoanalyzer. The capacities and cycle properties of the $Li_4Ti_5O_{12}$-SnO_2 composite powders were measured using 2032-type coin cells. The electrode was made of 40 mg of composite powders mixed with 5 mg of a carbon black and 5 mg of sodium carboxymethyl cellulose (CMC) in distilled water. Li metal and a polypropylene film were used as the counter electrode and the separator, respectively. The electrolyte was 1 M $LiPF_6$ mixed in a 1:1 volume ratio with ethylene carbonate/dimethyl carbonate (EC/DMC, Techno Semichem Co., Ltd., Korea). The entire cell was assembled in a glove box under an argon atmosphere. The electrochemical properties of the composite powders were measured using cycling in the range 0.1–2.5 V at various current densities.

3. RESULTS AND DISCUSSION

The morphologies of the powders prepared using spray drying process are affected by the preparation conditions as well as the types of spray solution used. In this study, tin oxalate was used instead of tin chloride (which, although it is the most popular source of tin, it is toxic) to avoid the corrosion of the spray drying apparatus. Clear aqueous solutions were prepared from both tin oxalate and TTIP. However, mixing the two solutions immediately formed a white precipitate. Citric acid was added to the tin oxalate solution in order to form tin citrate before mixing that solution with the TTIP one. Citric acid was used as the chelating agent that enabled the formation of a homogeneous solution of Sn, Ti, and Li components. The preparation conditions, such as the inlet and outlet temperatures of

the spray dryers, the flow rate of the drying gas, and the feed rate of the liquid, were optimized to prepare the spherical, hollow precursor powders of the $Li_4Ti_5O_{12}$-SnO_2 composite. Fig. 2 shows the SEM images of the precursor powders formed from the spray solutions with various Li contents. During spray drying process, neither decomposition of the metal salts nor evaporation of the metal components occurred because of the low temperature (below 350°C) and short residence time used to evaporate the water and form the dried precursor powders. The powders were unstable in high humidity air. Therefore, they were immediately fired to form the composite powders. Heat was evolved from abrupt decomposition of the metal chelate, and it increased the temperature of the powders above the set temperature of the electric furnace during the temperature rising step. Evaporation of some Li components occurred during firing of the precursor powders to form the $Li_4Ti_5O_{12}$-SnO_2 composite powders.

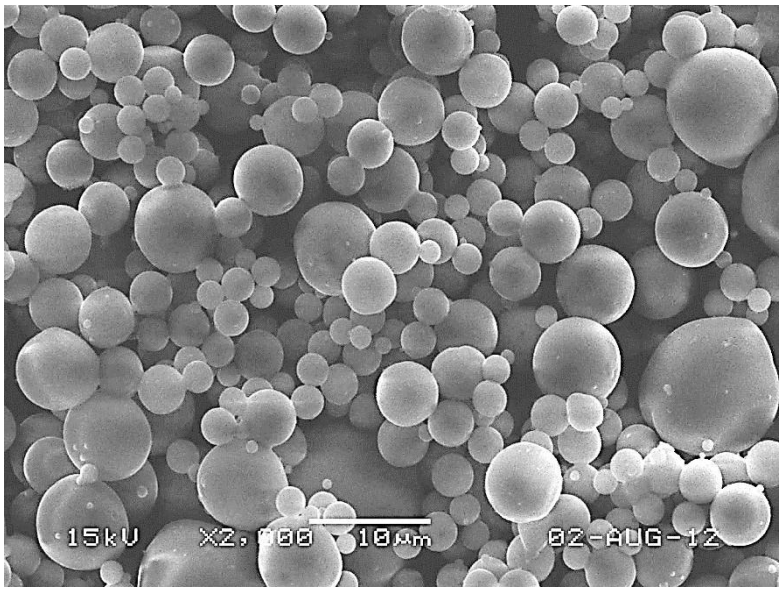

(a) Li 5% excess

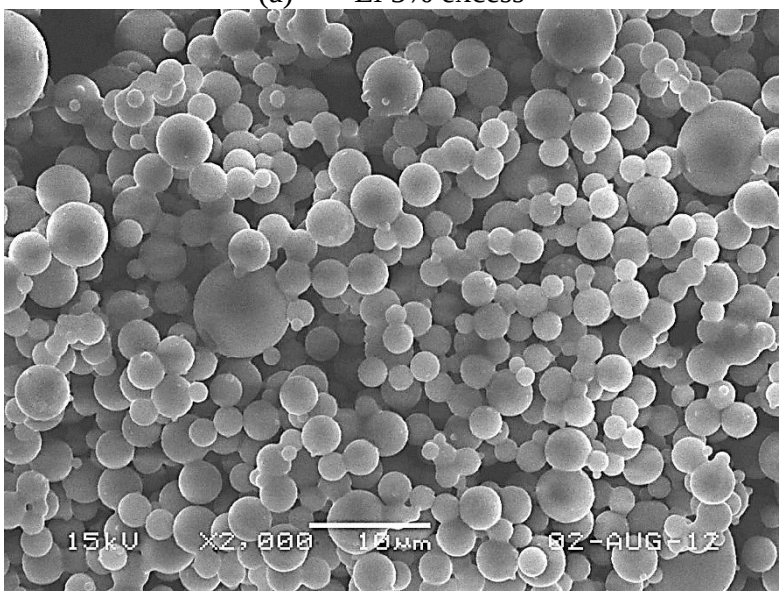

(b) Li 10% excess

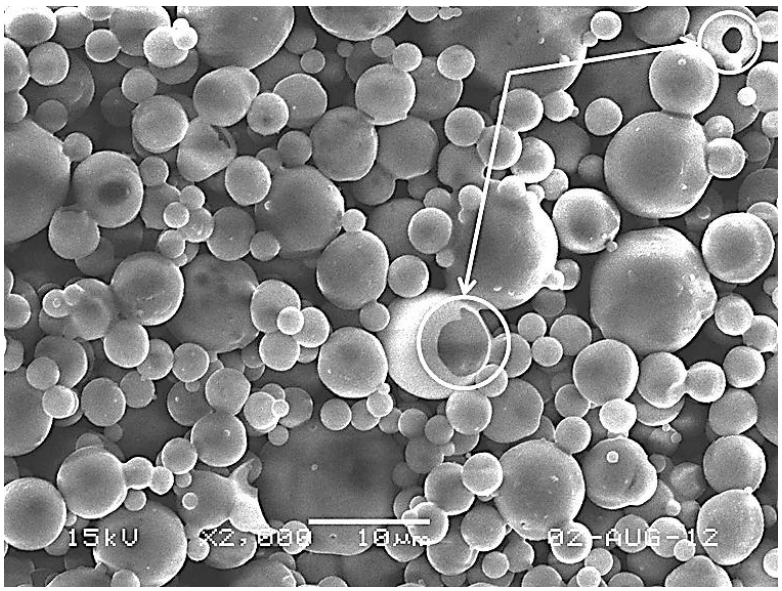

(c) Li 20% excess

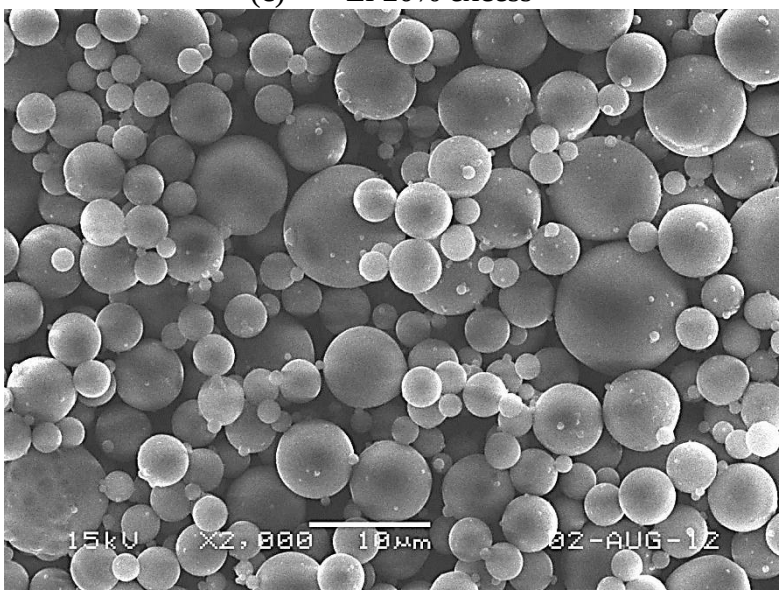

(d) Li 30% excess

Figure 2. SEM images of the precursor powders formed from the spray solutions with various Li contents.

Therefore, the precursor powders for $Li_4Ti_5O_{12}$-SnO_2 composite were formed from spray solutions containing various excess amounts of the Li component. The dried precursor powders were spherical and were several micrometers in diameter regardless of the excess amount of the Li component. The dried powders were also hollow, as shown by the arrows in Fig. 2.

Fig. 3 shows the TGA-DSC curves for the precursor powders obtained using spray drying process. The TGA curve for the precursor powders indicates three weight losses at temperatures below 400°C. The first prominent weight loss region from 40 to 150°C resulted from the loss of adsorbed water. The high weight loss from 160 to 400°C exhibited in the TGA curve for the precursor powders can be attributed to the decomposition of the metal salts and the carbon component. The total weight

loss of the precursor powders was 80%. The main exothermic peak associated with the decomposition of the metal salts and the carbon material was located at ~425°C in the DSC curve.

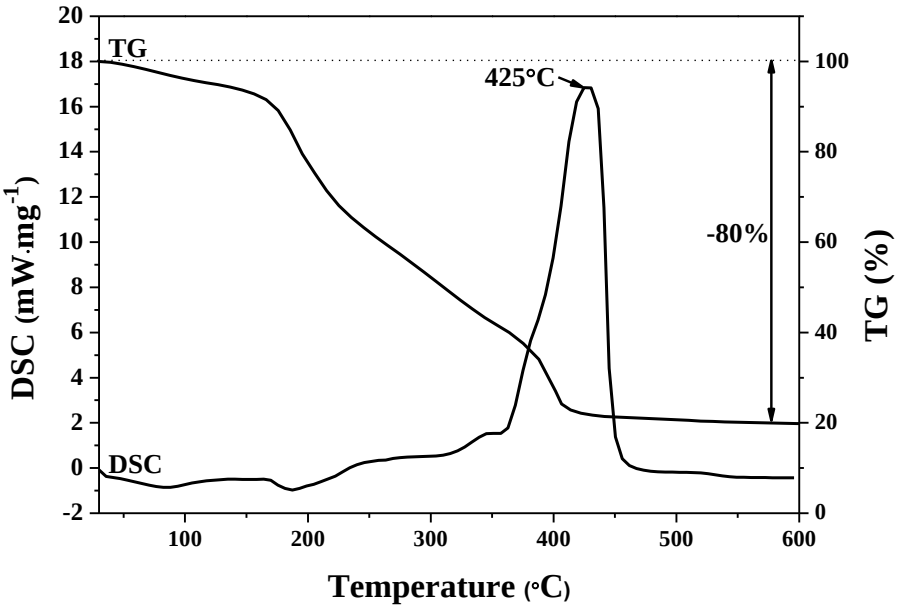

Figure 3. TG/DSC curves of the precursor powders obtained by spray drying process.

The morphologies of the $Li_4Ti_5O_{12}$-SnO_2 composite powders post-treated at 800°C in air are shown in Fig. 4. The composite powders were hollow spheres regardless of the excess amount of the Li component. Small holes formed by eruption of evaporated water vapor are observed in the composite powders, as shown by the arrows in Fig. 4. Fig. 5 shows the TEM image and dot-mapping images of the composite powders post-treated at 800°C. The excess amount of the Li component was 20 wt% of the stoichiometric amount used to form the $Li_4Ti_5O_{12}$-SnO_2 composite powders. The TEM and dot-mapping images of the composite powders show the two separate phases.

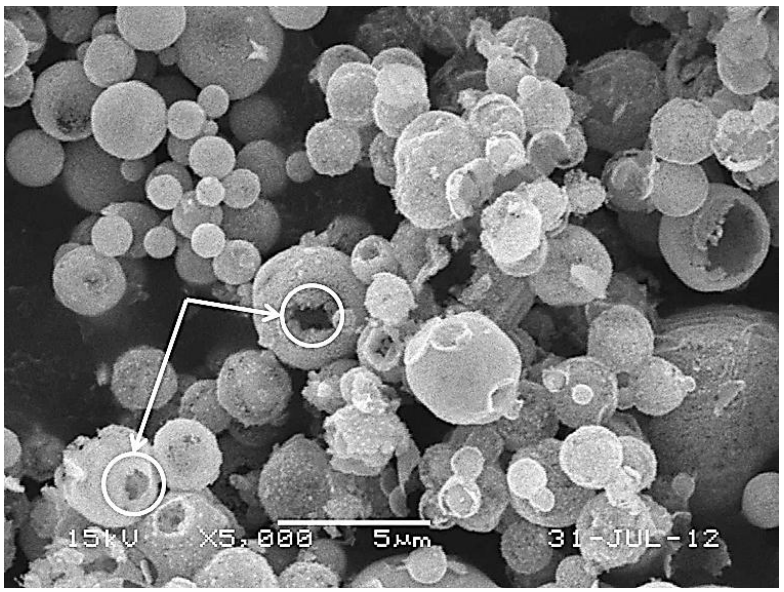

(a) Li 5% excess

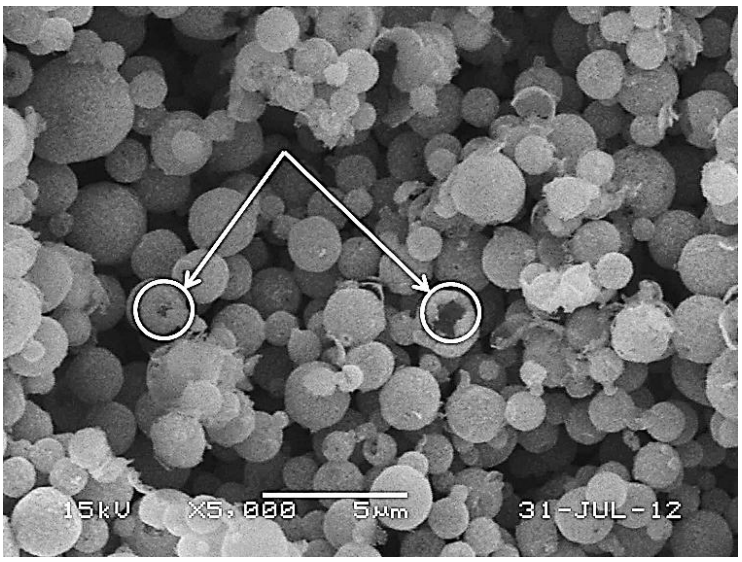

(b) Li 10% excess

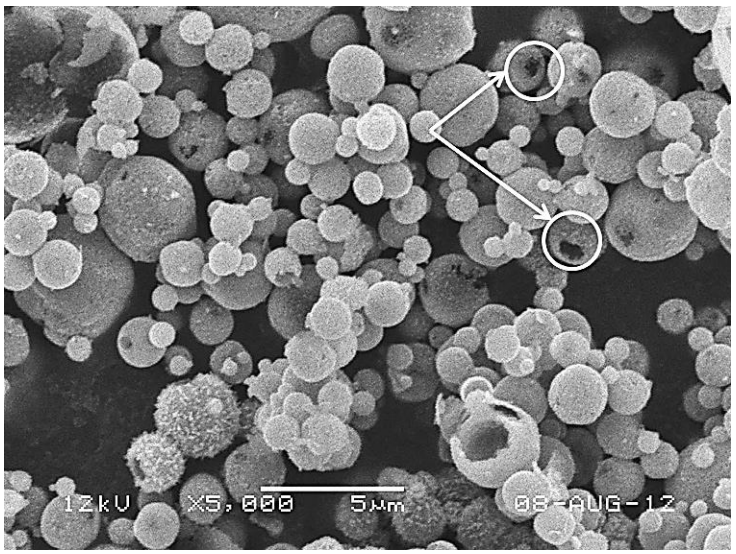

(c) Li 20% excess

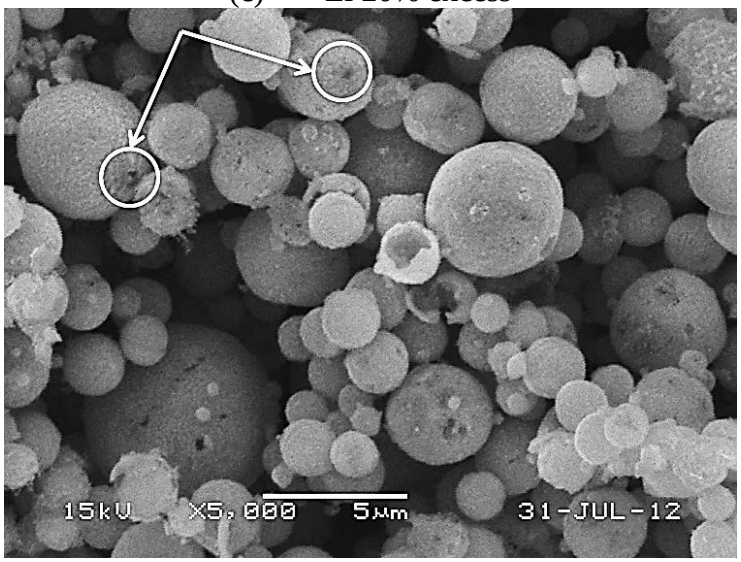

(d) Li 30% excess

Figure 4. SEM images of the post-treated $Li_4Ti_5O_{12}$-SnO_2 composite powders with various excess amount of the Li component.

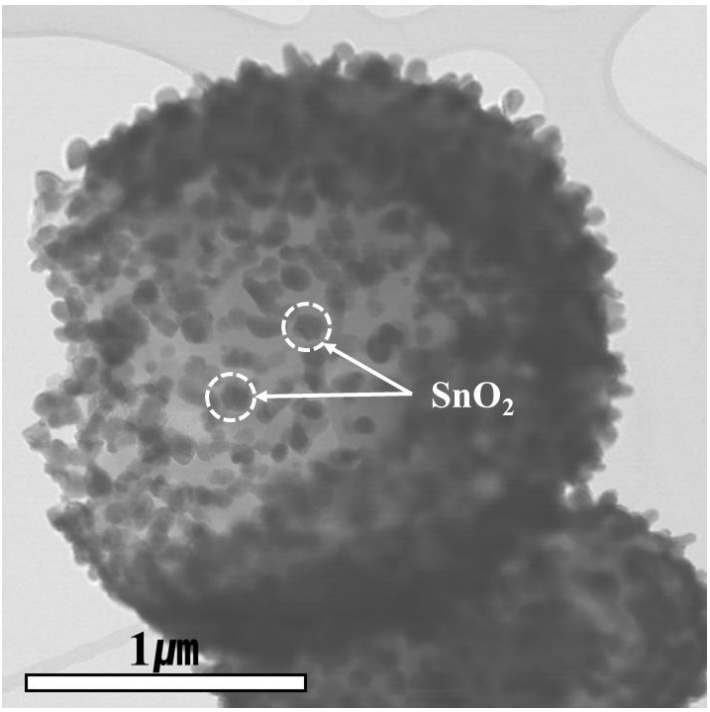

(a) low-resolution image

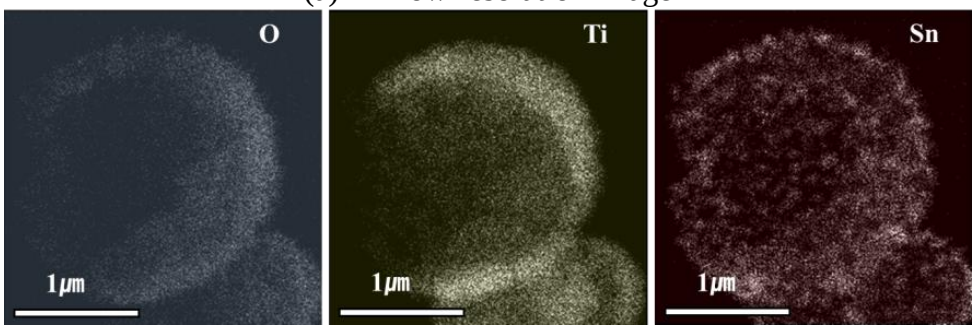

(b) dot mapping

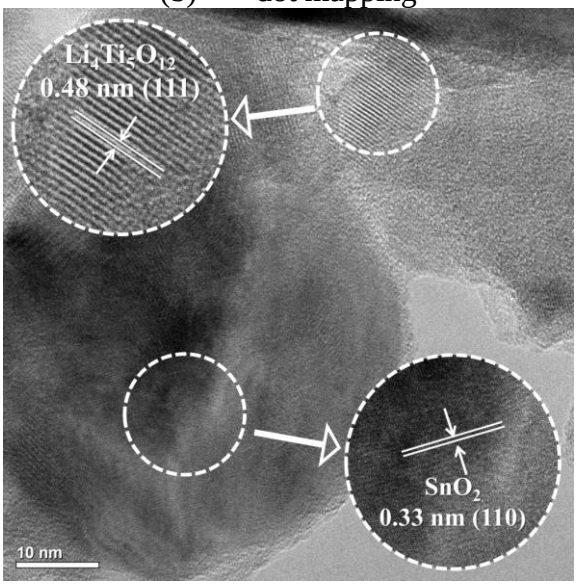

(c) high-resolution image

Figure 5. TEM images and results of dot mapping of the $Li_4Ti_5O_{12}$-SnO_2 composite powders post-treated at 800^oC.

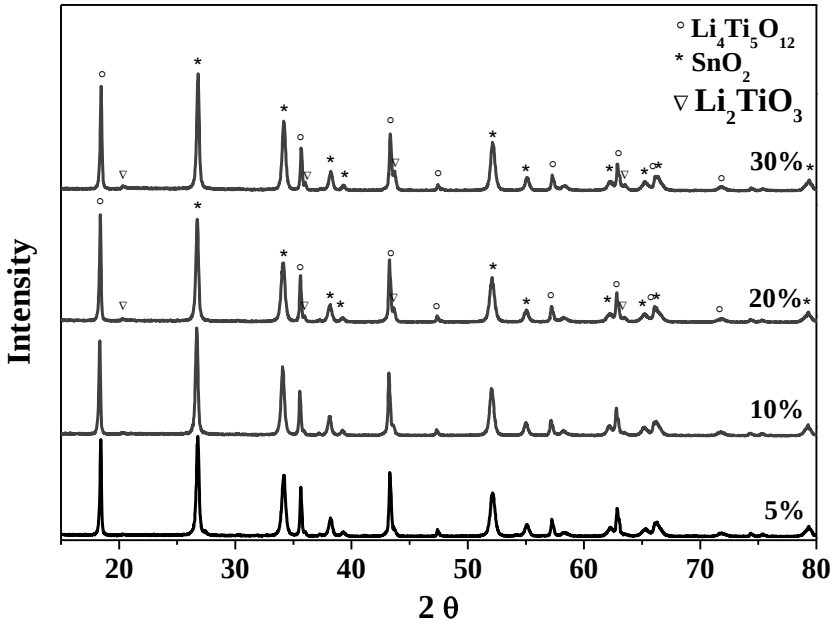

Figure 6. XRD patterns of the post-treated $Li_4Ti_5O_{12}$-SnO_2 composite powders with various excess amount of the Li component.

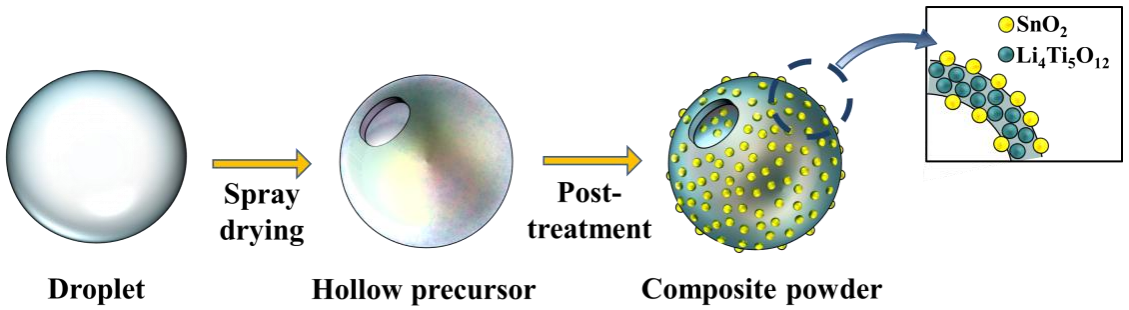

Figure 7. The schematic diagram of the formation process of the $Li_4Ti_5O_{12}$–SnO_2 composite powders in the spray drying method.

The Ti component is uniformly distributed throughout the composite powder; however, the Sn component forms a series of islands throughout the composite powders, as shown by the circles in the TEM image. The high-resolution TEM image of the composite powders exhibited clear lattice fringes separated by 0.48 and 0.33 nm. These values correspond to the (111) plane of $Li_4Ti_5O_{12}$ and the (110) plane of SnO_2. Fig. 6 shows the XRD patterns for the $Li_4Ti_5O_{12}$-SnO_2 composite powders post-treated at 800°C. The composite powders exhibited mixed crystal structures of $Li_4Ti_5O_{12}$ and SnO_2 phases regardless of the excess amount of the Li component. Small peaks associated with the Li-rich Li_2TiO_3 impurity phase were observed in the XRD patterns of the composite powders formed with high Li content. Tin oxide from the composite material did not affect the formation of the $Li_4Ti_5O_{12}$ phase. The precursor powders spray-dried from the homogeneous aqueous solution exhibited uniform distribution of the Li, Ti, and Sn components. The formation of the $Li_4Ti_5O_{12}$ and the SnO_2 phases during firing produced nanocomposite powders, as shown in the TEM images in Fig. 5. The mean crystallite sizes of

the $Li_4Ti_5O_{12}$ and SnO_2 crystals of the composite powders prepared with 20 wt% excess Li were calculated using the Scherrer equation as 100 and 42 nm, respectively.

Fig. 7 shows a schematic diagram of the formation of the $Li_4Ti_5O_{12}$-SnO_2 composite powders by spray drying process. One dried particle is formed from one droplet by complete evaporation of the water solvent. The metal salts precipitated from the liquid droplets by fast-drying exhibited poor permeability of evaporated water molecules. Therefore, the powder particles expanded and became hollow during water evaporation. Decompositions and reactions of Sn, Li, and Ti components occurred during post-treatment of the precursor powders in air to form the SnO_2 and $Li_4Ti_5O_{12}$ phases. Nanosized SnO_2 crystals were uniformly distributed throughout the hollow, spherical spinel $Li_4Ti_5O_{12}$ matrix. The mean size of the SnO_2 crystals in the composite powders as measured from the TEM image was 50 nm. The mean thickness of the hollow composite powders as measured from the TEM image was 100 nm.

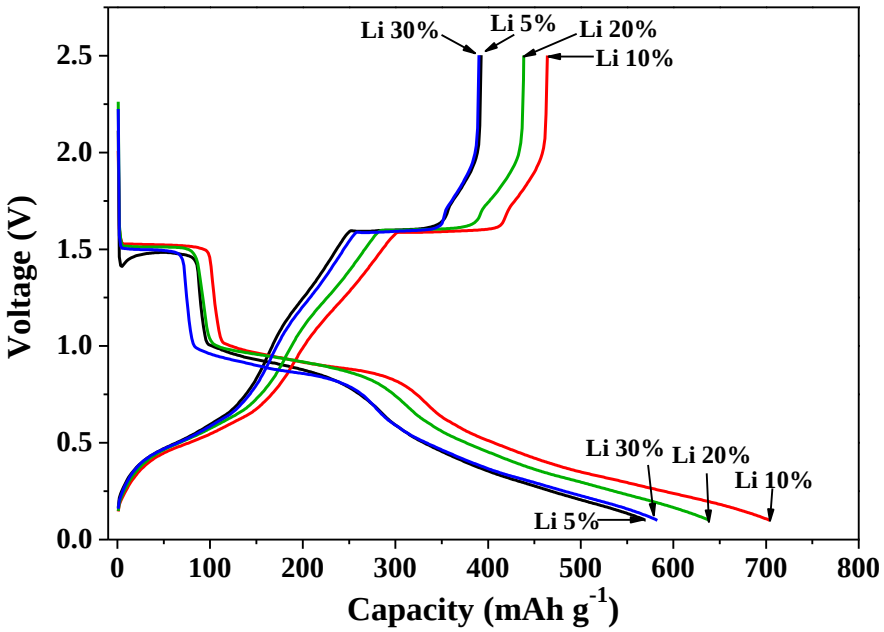

Figure 8. Initial charge/discharge curves of the post-treated $Li_4Ti_5O_{12}$-SnO_2 composite powders with various excess amount of the Li component.

Fig. 8 shows the initial charge and discharge curves for the $Li_4Ti_5O_{12}$-SnO_2 composite powders prepared with various excess amounts of the Li component, measured at room temperature at a constant current density of 170 mA g^{-1} between 0.1 and 2.5 V. In this work, Li insertion into anode electrode is referred to as "charge" and Li extraction is referred to as "discharge." The initial charge and discharge curves for the composite powders exhibited two distinct potential plateaus at ~1.5 and ~1.0 V during the first cycle regardless of the excess amount of the Li component. The two plateaus can be attributed to the corresponding reductions of Ti(IV) to Ti(III) and of Sn(IV) to Sn(0) [19-23]. During subsequent cycles (data not shown), potential plateaus at ~1.0 V are not observed. The potential plateau at ~1.0 V in the curve for the pure SnO_2 powders is only observed in the first charge

curve [24]. However, in the other charge curves, the lengths of the potential plateaus at ~1.5 V due to $Li_4Ti_5O_{12}$ are maintained during 20 cycles. The lengths of the potential plateaus at ~1.6 V in the discharge curves are also maintained during 20 cycles. The stable potential plateaus of the composite powders in the charge and discharge curves during cycling indicate the stability of the $Li_4Ti_5O_{12}$ phase. The decrease in the capacities of the composite powders during cycling resulted from the instability of the SnO_2 component.

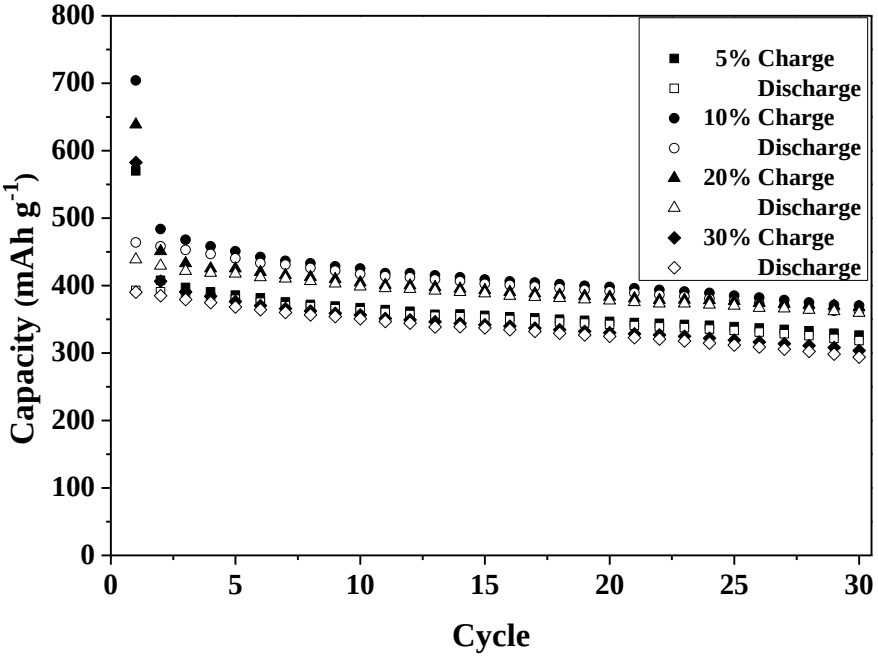

Figure 9. Cycling properties of the post-treated $Li_4Ti_5O_{12}$-SnO_2 composite powders with various excess amount of the Li component.

Fig. 9 shows the cycling properties of the composite powders prepared with various excess amounts of the Li component. The composite powders exhibited high first charge capacities and large irreversible capacity losses regardless of the excess amount of the Li component. The large irreversible capacity losses are mainly attributed to the high content of SnO_2 in the composite powders. Formation of Li_2O during the first charging cycle by the reaction of SnO_2 with Li caused a large initial lithiation capacity loss [24]. The composite powders prepared with 20 wt% excess Li exhibited high initial charge and discharge capacities, 639 and 439 mAh g^{-1}, respectively, in which the Coulombic efficiency was 69%. The discharge capacity of the composite powders prepared with 20 wt% excess Li decreased from 439 to 359 mAh g^{-1} by the 30th cycle, the capacity retention being 82%. The capacity retentions of the composite powders prepared with 5, 100, and 30 wt% excess Li after 30 cycles were 81, 79, and 75%, respectively. The $Li_4Ti_5O_{12}$-SnO_2 composite powders prepared with 10 and 20 wt% excess Li exhibited high discharge capacities, above 350 mAh g^{-1}, even after 30 cycles at a high current density of 170 mA g^{-1}. The presence of the SnO_2 phase increased the capacities and the conductivities of the composite powders. The presence of the main $Li_4Ti_5O_{12}$ phase improved the cycle properties of the composite powders by decreasing the degree of aggregation in the active Sn powders imbedded in

composite powder matrices. The stable $Li_4Ti_5O_{12}$ matrix and hollow inner structure of the composite powders also decreased the amount of internal stress due to changes in powder particle volume during Li intercalation and deintercalation [25-27].

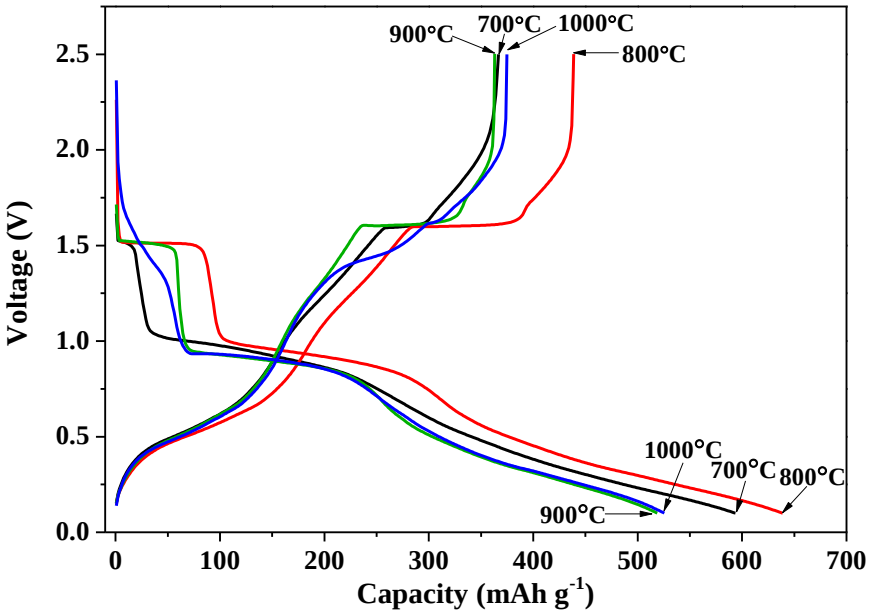

Figure 10. Initial charge/discharge curves of the $Li_4Ti_5O_{12}$-SnO_2 composite powders post-treated at various temperatures.

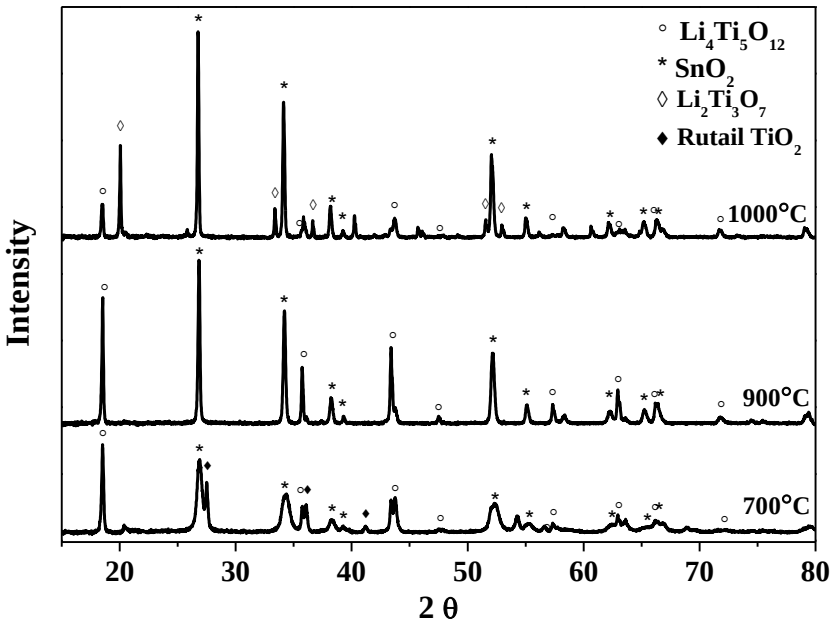

Figure 11. XRD patterns of the $Li_4Ti_5O_{12}$-SnO_2 composite powders post-treated at various temperatures.

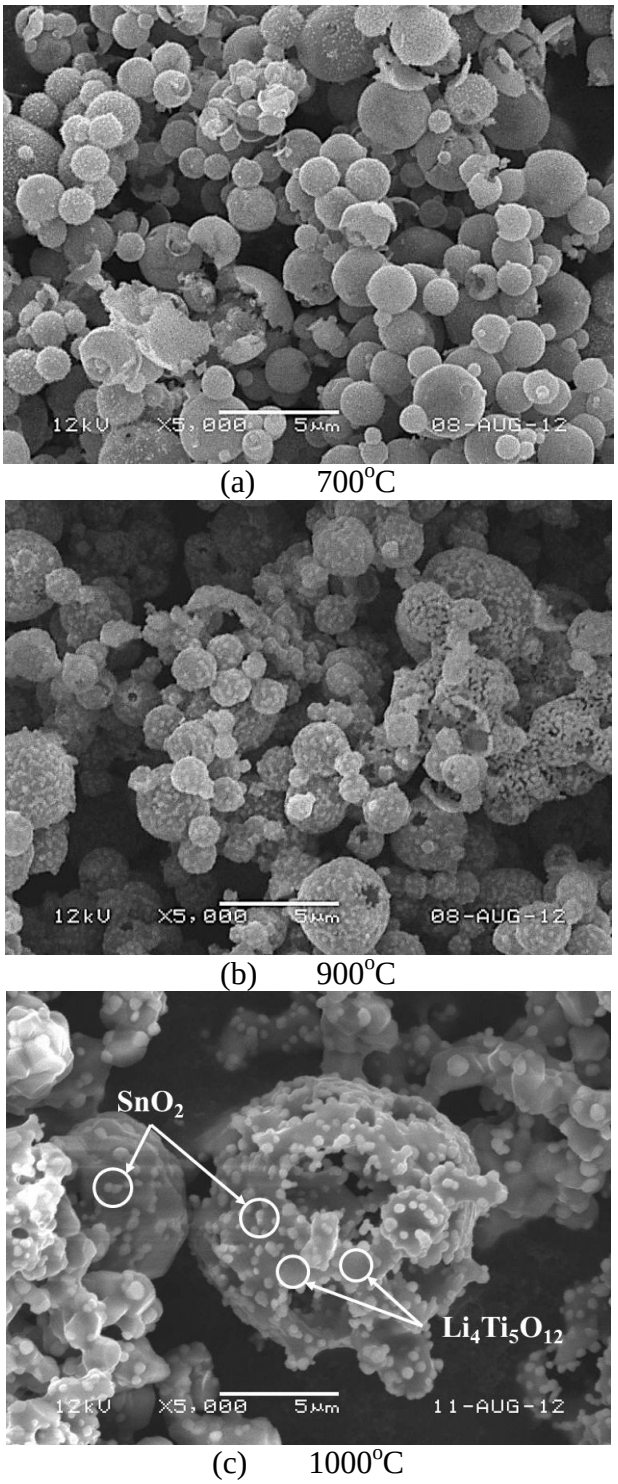

Figure 12. SEM images of the $Li_4Ti_5O_{12}$-SnO_2 composite powders post-treated at various temperatures.

Fig. 10 shows the initial charge and discharge curves for the $Li_4Ti_5O_{12}$-SnO_2 composite powders post-treated at temperatures between 700 and 1000°C. The curves for composite powders exhibited similar shapes for the initial charge and discharge curves regardless of the post-treatment temperatures. However, the two distinct plateaus at ~1.5 and ~1.0 V were only observed in the first

charge curves for the composite powders post-treated at 800 and 900°C. The initial charge and discharge curves for the composite powders post-treated at 800°C exhibited the highest initial charge and discharge capacities. Fig. 11 shows the XRD patterns for the composite powders post-treated at various temperatures. The patterns for the composite powders post-treated at 700°C exhibited main crystal peaks associated with the $Li_4Ti_5O_{12}$, SnO_2, and TiO_2 phases as well as small peaks associated with impurity phases. Slight decomposition of the $Li_4Ti_5O_{12}$ composite powder crystals occurred at a high post-treatment temperature of 1000°C, forming the $Li_2Ti_3O_7$ impurities [28,29]. Fig. 12 shows the morphologies of the composite powders post-treated at various temperatures. The phase separation of the composite powders increased with increasing post-treatment temperature due to crystal growth of each phase, as shown in Figs. 4 and 12. The composite powders post-treated at 1000°C exhibited an aggregated, non-spherical structure. The composite powders post-treated at 800°C exhibited the highest capacities and good cycle properties because of phase purity, compositional homogeneity, and unique morphology.

4. CONCLUSIONS

Microstructure-controlled $Li_4Ti_5O_{12}$-SnO_2 composite powders were prepared by post-treating precursor powders obtained by spray-drying. Citric acid was used as the chelating agent to enable the formation of homogeneous solutions of Sn, Ti, and Li components. The preparation conditions of the spray dryer were optimized to prepare the spherical, hollow precursor powders of the $Li_4Ti_5O_{12}$-SnO_2 composite. The post-treated composite powders exhibited mixed crystal structures and hollow spheres, and the SnO_2 component was highly dispersed throughout the $Li_4Ti_5O_{12}$ matrix. The stable potential plateaus exhibited in the charge and discharge curves for the composite powders as measured during cycling indicate the stability of the $Li_4Ti_5O_{12}$ phase. The slight decrease in the capacities of the composite powders during cycling resulted from the instability of the SnO_2 component. The composite powders prepared with 20 wt% excess Li exhibited high initial charge and discharge capacities and good cycling because of their phase purity, compositional homogeneity, and unique morphology.

ACKNOWLEDGEMENT
This work was supported by the National Research Foundation of Korea (NRF) grant funded by the Korea government (MEST) (No. 2012R1A2A2A02046367).

References

1. S. Venkatraman, J. Choi, A. Manthiram, *Electrochem. Commun*., 6 (2004) 832.
2. Z. Lu, D.D MacNeil, J.R. Dahn, *Electrochem. Solid-State Lett*., 4 (2001) A200.
3. S.H. Huang, Z.Y. Wen, J. Zhang, Z. Gu, X. Xu, *Solid State Ionics*, 177 (2006) 851.
4. S.H. Huang, Z.Y. Wen, B. Lin, J.D. Han, X.G. Xu, *J. Alloys Compd.*, 457 (2008) 400.
5. S.H. Huang, Z.Y. Wen, X.J. Zhu, X.L. Yang, *J. Electrochem. Soc.*, 152 (2005) A1301.
6. J. Gao, C.Y. Jiang, C.R. Wan, *J. Electrochem. Soc.*, 157 (2010) K39.
7. L.Z Xing, Z.Q. He, Z.L. Yin, Q.Y. Chen, *Trans. Nonferrous Met. Soc. China*, 20 (2010) s267.

8. Y.Y. Wang, Y.J. Hao, Q.Y. Lai, J.Z. Lu, Y.D. Chen, X.Y. Ji, *Ionics*, 14 (2008) 85.
9. A. Sivashanmugam, S. Gopukumar, R. Thirunakaran, C. Nithya, S. Prema, *Mater. Res. Bull*., 46 (2011) 492.
10. X.W. Lou, M.L. Chang, L.A. Archer, *Adv. Mater*., 21 (2009) 2536.
11. W.M. Zhang, J.S. Hu, Y.G. Guo, S.F. Zheng, L.S. Zhong, W.G. Song, L.J. Wan, *Adv. Mater*., 20 (2008) 1160.
12. Z. Wang, L. Zhou, X.W. Lou, *Adv. Mater*., 24 (2012) 1903.
13. H.B. Wu, J.S. Chen, H.H. Hng, X.W. Lou, *Nanoscale*, 4 (2012) 2526.
14. C. Jiang, Y. Zhou, I. Honma, T. Kudo, H. Zhou, *J. Power Sources*, 166 (2007) 514.
15. S.J. Han, B.C. Jang, T.A. Kim, S.M Oh, T.H. Hyeon, *Adv. Funct. Mater*., 15 (2005) 1845.
16. Y. Yu, C.H. Chen, Y. Shi, *Adv. Mater*., 19 (2007) 993.
17. M.S. Park, G.X. Wang, Y.M. Kang, D. Wexler, S.X. Dou, H.K. Liu, *Angew. Chem. Int. Ed*., 46 (2007) 750.
18. Y. Wang, J.Y. Lee, H.C. Zeng, *Chem. Mater.*, 17 (2005) 3899.
19. A.S. Aricò, P. Bruce, B. Scrosati, J.M. Tarascon, W.V. Schalkwijk, *Nature Mater*., 4 (2005) 366.
20. D. Peramunage, K.M. Abraham, *J. Electrochem. Soc*., 145 (1998) 2609.
21. M. Winter, J.O. Besenhard, *Electrochim. Acta*, 45 (1999) 31.
22. D.W. Kim, I.S. Hwang, S.J. Kwon, H.Y. Kang, K.S. Park, Y.J. Choi, K.J. Choi, J.G. Park, *Nano Lett*., 7 (2007) 3041.
23. I.A. Courtney, J.R. Dahn, *J. Electrochem. Soc.*, 144 (1997) 2943.
24. I.A. Courtney, J.R. Dahn, *J. Electrochem. Soc.*, 144 (1997) 2045.
25. T. Ohzuku, A. Ueda, N. Yamamoto, *J. Electrochem. Soc*., 142 (1995) 1431.
26. T. Ohzuku, A. Ueda, N. Yamamoto, Y. Iwakoshi, *J. Power Sources*, 54 (1995) 99.
27. J. Huang, Z. Jiang, *Electrochem. Solid-State Lett*., 11 (2008) A116.
28. H.A. Mosqueda, H. Pfeiffer, *Process. Applic. Ceram*., 5 (2011) 199.
29. M. Picquart, L. Escobar-Alarcón, E. Torres, T. Lopez, E. Haro-Poniatowskiez, *J. Mater. Sci*., 37 (2002) 3241.